# Plane-grating monochromator at BESSY II using collimated light

## R. Follath,* F. Senf and W. Gudat

*BESSY, Lentzeallee 100, 14195 Berlin, Germany.
E-mail: follath@exp.bessy.de*

At the German synchrotron radiation facility BESSY II, the VUV photon energy range between 15 and 600 eV is covered by the first, third and fifth harmonics of the U125 undulator. The beamline connected to this source is a plane-grating monochromator (PGM) with a variable deviation angle. The plane grating is illuminated by collimated radiation, allowing very flexible use of the monochromator. Depending on users' demands, it can be operated at high spectral resolution, high-order suppression or in high-flux mode, simply by software control.

**Keywords: plane gratings; monochromators; collimated light.**

## 1. Introduction

In this report we describe the plane-grating monochromator (PGM), which is installed at the undulator U125 (U125-PGM). It has to be a general-purpose instrument to cope with the very different user requests. For this purpose, we chose a plane-grating monochromator with a variable deviation angle, based on the well known SX700 monochromators at BESSY I. Over the past 15 years, this type of monochromator has proved to be a very successful, flexible and easy-to-use instrument (Petersen *et al.*, 1995). The main restriction of this instrument is its confinement to a special value of the so-called fixed-focus constant $c_{ff}$. It is defined as $c_{ff} = -\cos^2 \beta / \cos^2 \alpha$, where $\alpha$ is the incident and $\beta$ the diffracted angle measured to the normal of the grating surface. As a consequence of the focusing property of the plane grating, the fixed-focus constant is fixed for such a monochromator after its optical design period. It is possible to overcome this restriction if bending mirrors or movable slits are used. A more elegant way, which avoids mechanical problems and instabilities, is the illumination of the grating with collimated light. In this case, the accessible $c_{ff}$ values are only limited by the rotation angles of the plane mirror and the grating.

The optical design is thus similar to that of conventional crystal monochromators for hard X-rays; several monochromators in the past also took advantage of collimated light in the soft X-ray regime (Howells, 1980; Hunter *et al.*, 1982; Naletto & Tondello, 1992).

During operation, the behaviour of the monochromator can be adapted to meet the user's demands conveniently without moving slits or bending mirrors. It can be tuned for high spectral resolution, high photon flux or for good spectral purity (Follath & Senf, 1997). It is possible to limit the contributions of the higher orders to a value below 5% over the whole energy range by a proper variation of the $c_{ff}$ values at the grating.

**Table 1**
BESSY II parameters (r.m.s. values) in the long straight sections for a coupling of 3%.

| | |
|---|---|
| Horizontal source size ($\sigma_e^x$) | 310 μm |
| Horizontal source divergence | 17 μrad |
| Vertical source size ($\sigma_e^y$) | 21 μm |
| Vertical source divergence | 7.1 μrad |

**Table 2**
Characteristics of the insertion device U125 for a minimum magnetic gap of 20 mm; the tuning range of the monochromator is shown in Fig. 2.

| | |
|---|---|
| Period $\lambda$ (mm) | 125 |
| Number $N$ | 32 |
| First harmonic $E$ (ev) | 11–95 |
| Third harmonic $E$ (ev) | 160–439 |
| Fifth harmonic $E$ (ev) | 267–595 |

## 2. The source

The monochromator is situated at the U125 undulator. The properties of the storage ring in this high-$\beta$ section H13 are given in Table 1, the characteristics of the undulator source in Table 2. As in the common Petersen design of PGMs, the monochromator operates without an entrance slit and uses the undulator source instead. For a proper estimation of the monochromator performance, it is thus essential to take into account the properties of the source. This has been performed in two steps. First, we used the program *SMUT* (Jacobsen & Rarback, 1985) to calculate the photon-flux distribution at a distance of 10 m. In the second step, the ray-trace program *RAY* (Schäfers, 1996) was used to define a volume from which the rays originate. With this, the ray-trace program generates an angular distribution according to the given *SMUT* file. The lateral source size of this volume $\sigma_{tot}$ was estimated as a convolution of the electron-beam size $\sigma_e$ and the coherent undulator source size $\sigma_p = (\lambda L/4\pi)^{1/2}$ (Padmore & Warwick, 1994) with the values for the vertical and horizontal electron-beam sizes, respectively. The effective length of the undulator source was set to zero.
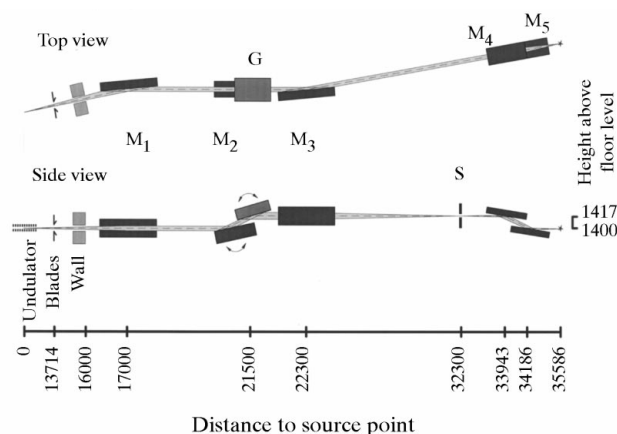


**Figure 1**
The optical layout of the beamline (all dimensions are in mm). $M_1$ is a toroidal mirror which collimates the light in the horizontal and vertical directions. The plane mirror $M_2$ is used to vary the deviation angle at the plane grating G. Vertically, the diffracted light is focused onto the exit slit by the cylindrical mirror $M_3$. The subsequent refocusing is performed by the mirrors $M_4$ and $M_5$ in the vertical and horizontal directions, respectively.

**Table 3**
Parameters of the optical elements.

The slope errors are r.m.s. values in the meridional/sagittal directions (if different); $R$ is the large meridional radius, $\rho$ is the sagittal one, both in mm; the grating parameter $N$ is the line density; $t$ and $w$ are, respectively, the line depth and the valley to spacing ratio.

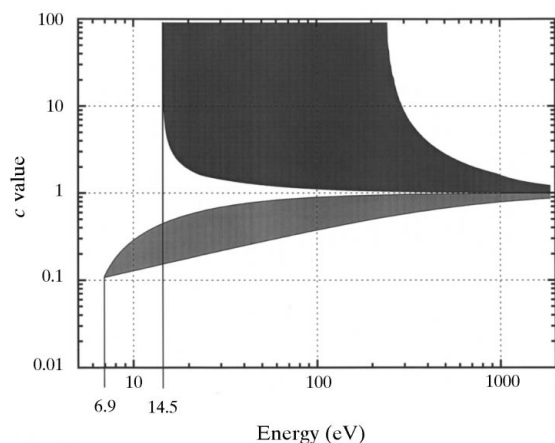| Component | Shape | Slope errors ($''$) | Parameter | Deviation angle ($°$) | Size [length (mm) × width (mm)] |
|---|---|---|---|---|---|
| $M_1$ | Toroidal | 1 | $R = 650\ 000$ $\rho = 1779$ | 174 | $200 \times 25$ |
| $M_2$ | Plane | 0.1 | | 169–188 | $300 \times 30$ |
| $M_3$ | Cylindrical | 1 | $\rho = 1047$ | 174 | $230 \times 40$ |
| $M_4$ | Spherical | 0.5/2 | $R = 47\ 080$ | 176 | $110 \times 40$ |
| $M_5$ | Cylindrical | 1/3 | $\rho = 97.9$ | 176 | $110 \times 40$ |
| $G_1$ | Plane | 0.1 | $N = 300$ lines mm$^{-1}$ $t = 36$ nm $w = 0.57$ | 169–188 | $100 \times 20$ |
| $G_2$ | Plane | 0.1 | $N = 1200$ lines mm$^{-1}$ $t = 10$ nm $w = 0.67$ | 169–188 | $100 \times 20$ |

## 3. The beamline

The optical layout of the beamline is shown in Fig. 1; the data of the mirrors and gratings are given in Table 3. Four water-cooled blades allow a beam to be formed inside the radiation-shielding wall. They are part of the front-end and can be set by the monochromator control to cut off the off-axis radiation from the central undulator cone.

The horizontally deflecting mirror $M_1$ collimates the light in the horizontal and vertical directions. Besides this optical function, it separates the U125-PGM beamline from a second branch, dedicated to an SGM (spherically grating monochromator) and additionally absorbs most of the unwanted higher harmonics of the undulator. Since its deflection plane is perpendicular to the dispersion plane of the subsequent grating, surface distortions caused by the high heat load and slope errors do not deteriorate the resolving power of the monochromator. They are suppressed by a factor $\sin\varphi$ where $\varphi$ is the grazing incidence angle (Cash, 1987).

The plane mirror $M_2$ is used to vary the deviation angle at the grating G. Two laminar gratings with 300 and 1200 lines mm$^{-1}$ cover the energy ranges 20–600 and 80–2400 eV at a $c_{ff}$ of 2.25.

Because of the illumination of the grating with parallel light, we can vary the $c_{ff}$ value arbitrarily without defocusing. Fig. 2 shows the plot of $c_{ff}$ versus energy for the 300 lines mm$^{-1}$ grating and indicates the accessible areas.
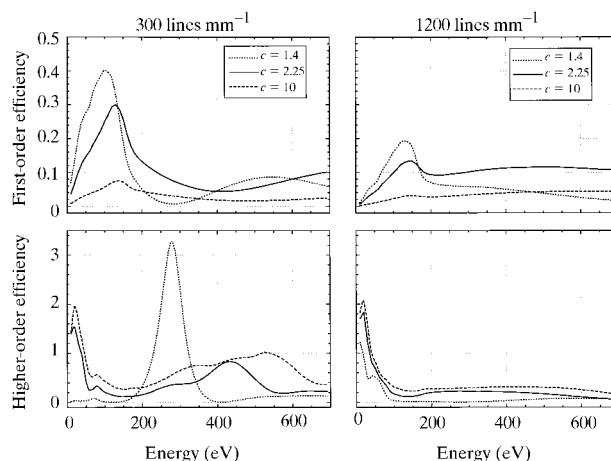
The horizontally deflecting mirror $M_3$ focuses the light in the vertical plane onto the exit slit S. Behind the slit a decoupled refocusing optic is used to form an image at the sample position. The focal length of the last mirror is 1400 mm, which should leave enough free space even for extended end-stations. The photon beam remains horizontal, a feature which considerably facilitates the alignment of experimental set-ups.

Because of the high heat load, the mirrors $M_1$ and $M_2$ as well as the gratings G are water cooled by a side cooling via copper blocks.

## 4. Expected performance

For a quantitative performance description, calculations were carried out using the computer programs *RAY* and *REFLEC* (Schäfers & Krumrey, 1996). The grating efficiencies $e_i(E)$ of the $i$th diffraction order at the photon energy $E$ were evaluated by using the code of Neviere *et al.* (1974).

Fig. 3 shows the grating efficiencies of the two gratings in the first diffracted order as well as the contribution of higher orders $f(E)$. The higher-order contributions were estimated according to $f(E) = \sum_{i=2}^{5} e_i(iE)/e_1(E)$. We find a good overall grating efficiency for a $c_{ff}$ value of 2.25. The contribution of the higher diffraction orders is reduced for $c_{ff} = 1.4$, except in the range between 200 and 300 eV, where the first-order efficiency has a minimum.



**Figure 2**
A map of the accessible $c_{ff}$ values ($c_{ff} = \cos^2\beta/\cos^2\alpha$) of the grating with 300 lines mm$^{-1}$. The dark shaded area shows the region of the first inside diffraction order ($c_{ff} > 1$), the light shaded area the region of the first outside diffraction order ($c_{ff} < 1$).



**Figure 3**
Grating efficiencies and higher-order contributions of the two gratings for three selected $c_{ff}$ values. The higher-order contributions $f(E)$ are approximated by $f(E) = \sum_{i=2}^{5} e_i(iE)/e_1(E)$.
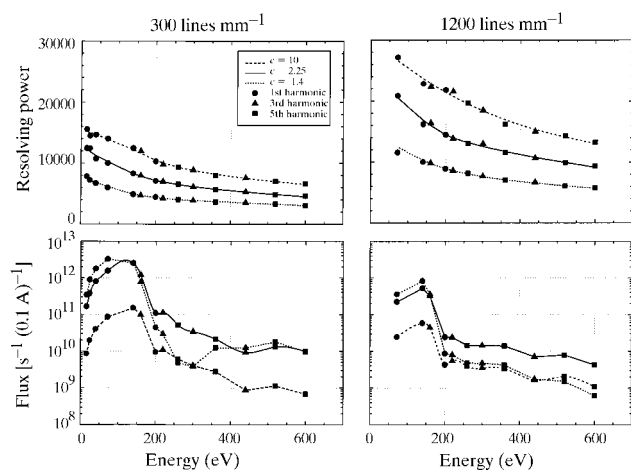
**Figure 4**
The calculated resolving power and associated flux of the beamline for an exit slit setting of 20 µm.

The resolving power, the related photon flux and the spot size were calculated for various undulator settings. In calculating the resolving power, the illumination of the grating had to be taken into account. For this we calculated the number of illuminated lines $N_l$ of the grating. The maximum resolving power due to the diffraction limit is then given by $(E/\Delta E)_l = 1/(N_l k)$ where $k$ is the diffraction order. Geometrical ray trace programs do not take account of this term. To include it in our calculations, we added it quadratically to the resolving power given by *RAY*.

The diffraction limit sets an upper theoretical limit to the resolving power, particularly for the 300 lines mm$^{-1}$ grating at low $c_{ff}$ values. Fig. 4 shows the results for the resolving power $E/\Delta E$ and the photon flux at this resolution. With a slit setting of 20 µm a resolving power of more than 10 000 can be obtained over the whole energy range. The photon flux reaches a maximum value of $5 \times 10^{12}$ s$^{-1}$ (0.1 A)$^{-1}$ at 100 eV. The reflectivity of the gold coatings causes a drop-off in the flux curves at 200 eV.

At this slit setting the spot size is approximately $70 \times 40$ µm (horizontal × vertical) FWHM (full width at half-maximum). The horizontal image size remains constant for all energies; the vertical increases from the minimum value of 40 µm proportional to the exit slit width. The beam divergence at the sample position depends on the energy and the $c_{ff}$ setting. It is about $1 \times 6$ mrad$^2$ for $c_{ff}$ = 2.25 at 140 eV and increases with the $c_{ff}$ value. The energy dependence is due to the angular distribution of the undulator radiation and is thus proportional to $1/(E^{1/2})$.

### References

Cash, W. (1987). *Appl. Opt.* **26**, 2915–2920.
Follath, R. & Senf, F. (1997). *Nucl. Instrum. Methods A*, **390**, 388–394.
Howells, M. R. (1980). *Nucl. Instrum. Methods*, **177**, 127–139.
Hunter, W. R., Williams, R. T., Rife, J. C., Kirkland, J. P. & Kabler, M. N. (1982). *Nucl. Instrum. Methods*, **195**, 141–153.
Jacobsen, C. & Rarback, H. (1985). *SPIE J.* **582**, 201–212.
Naletto, G. & Tondello, G. (1992). *Pure Appl. Opt.* **1**, 347–358.
Neviere, M., Vincent, P. & Petit, R. (1974). *Nouv. Rev. Opt.* **5**, 65.
Padmore, H. A. & Warwick, T. (1994). *J. Synchrotron Rad.* **1**, 27–36.
Petersen, H., Jung, C., Peatman, W. B. & Gudat, W. (1995). *Rev. Sci. Instrum.* **66**, 1–14.
Schäfers, F. (1996). *BESSY Tech. Ber.* **202/96**, 1–34.
Schäfers, F. & Krumrey, M. (1996). *BESSY Tech. Ber.* **201/96**, 1–17.